



HAL
open science

Interface crack initiation at V-notches along adhesive bonding in weakly bonded polymers subjected to mixed-mode loading

Van-Xuan Tran, Dominique Leguillon, Arun Krishnan, Luoyu Roy Xu

► **To cite this version:**

Van-Xuan Tran, Dominique Leguillon, Arun Krishnan, Luoyu Roy Xu. Interface crack initiation at V-notches along adhesive bonding in weakly bonded polymers subjected to mixed-mode loading. International Journal of Fracture, 2012, 176 (1), pp.65-79. 10.1007/s10704-012-9727-x . hal-04794165

HAL Id: hal-04794165

<https://hal.science/hal-04794165v1>

Submitted on 29 Dec 2024

HAL is a multi-disciplinary open access archive for the deposit and dissemination of scientific research documents, whether they are published or not. The documents may come from teaching and research institutions in France or abroad, or from public or private research centers.

L'archive ouverte pluridisciplinaire **HAL**, est destinée au dépôt et à la diffusion de documents scientifiques de niveau recherche, publiés ou non, émanant des établissements d'enseignement et de recherche français ou étrangers, des laboratoires publics ou privés.



Distributed under a Creative Commons Attribution - NonCommercial 4.0 International License

Interface crack initiation at V-notches along adhesive bonding in weakly bonded polymers subjected to mixed-mode loading

V. -X. Tran, D. Leguillon, A. Krishnan, L. R. Xu

Abstract In this paper, interface crack initiation at V-notches along adhesive in bonded Polycarbonate (PC) and Poly Methyl Methacrylate (PMMA) subjected to mixed-mode loading conditions was investigated based on a combined experimental, finite element and matched asymptotic analysis. The V-notch specimens with an adhesive interface starting from its tip made at different notch angles were tested under three-point bending conditions. The experimental observations show that the specimens mainly fail by cracks along the interface. Also, the load at the crack initiation increases when the notch angle increases. The computational results are then used to explain and to correlate with the experimental data. A two-fold criterion developed by Leguillon (Eur J Mech A/Solids 21:61–72 2002) that requires a simultaneous satisfaction of both Griffith energy and stress conditions for the crack initiation at a notch in the specimen made of a homogeneous brittle material is first extended for

V-notch specimens under mixed-mode loading conditions and then used to estimate the crack initiation load. The estimated loads appear to agree well with the experimental data. Finally, an inverse method is proposed to estimate the values of fracture toughness at different mode mixity ratios.

Keywords V-notch specimen · Adhesive bonding · Strength · Fracture toughness · Matched asymptotic analysis · Finite element analysis · Fracture criterion

1 Introduction

Stress concentrations are due to the geometry such as corners, sharp notches and re-entrant angle, and to the mismatch between material properties at the interface between two different materials. It should be noted that locations of stress concentrations are mainly the weakest sites for crack initiation. A thorough investigation of the failure of specimens containing locations of stress concentration is therefore important to improve the structure integrity. As an example, fracture and failure in brittle homogenous materials containing V-notches have been extensively investigated, in Dunn et al. (1997a), Dunn et al. (1997b), Leguillon (2002), Leguillon and Yosibash (2003a), Leguillon and Yosibash (2003b), Yosibash et al. (2004), Yosibash et al. (2006) and Priel et al. (2007), Gomez et al. (2009).

Recently, composite materials are widely used in the aircraft industry for the construction of civilian carriers.

V.-X. Tran · D. Leguillon (✉)
Institut Jean Le Rond d'Alembert, CNRS UMR7190,
Université Pierre et Marie Curie, 4 place Jussieu,
75005 Paris, France
e-mail: dominique.leguillon@upmc.fr

A. Krishnan
Department of Civil and Environmental Engineering,
Vanderbilt University, Nashville, TN 37235, USA

L. R. Xu
Department of Mechanical Engineering, University of Texas,
El Paso, TX 79968, USA

These composite parts complete the metal structures that are mostly made of aluminum. The joining of the aluminum parts to the composite parts is traditionally done by rivets. However, the riveting is an invasive process that adds weights to the airplane, creates weak points and increases the labor cost as well. Therefore, alternative joining processes should be explored. Recently, the adhesive bonding becomes a promising joining process that the aerospace manufacturers plan to replace the riveting. The study of strength and fracture toughness of the adhesive bonding is critical to ensure the integrity of structural components. It should be noted that most of the current literature is for cracked specimens joint by adhesive bonding as summarized in Krishnan and Xu (2011a,b). It is pointed out that the singular behavior of the stress solution at a V-notch is quite different from that at a crack tip (Xu et al. 2004a). Also, most of the fracture process of the adhesive joint specimens is brittle. Therefore, the crack initiation at V-notches along the adhesive bonding needs to be explored in order to develop robust prediction models for an optimal manufacturing of the adhesive joints. The previously mentioned authors mainly addressed the failure of homogeneous samples, rupture is characterized by a critical load and a cracking direction when considering complex loadings. The newly created crack essentially grows in mode I and only mode I toughness and tensile strength are involved. The originality of the present work lies in the fact that the crack is driven by the adhesive bond and grows under mixed modes I+II with references to mode I and II toughnesses as well as tensile and shear strengths.

In this research project, the crack initiation at V-notches along the adhesive bonding in specimens of two identical polymer parts and between aluminum and polymer parts is studied based on a combined experimental, finite element (FE) and matched asymptotic (MA) analysis. The results for V-notch specimens of bonded identical polycarbonate (PC) and Poly Methyl Methacrylate (PMMA) are reported in this paper while the results for V-notch specimens of different materials will be reported in a future paper. In this investigation, the originality of the experimental approach comes from the design of the specimen combining two parts with customized geometries that are bonded to create a sharp V-notch with an adhesive interface starting from its root. The V-notch specimens with different notch angles are tested under three-point bending conditions. The crack initiation loads and the equivalent stiffness of the speci-

mens are obtained from the experiments (Krishnan and Xu 2012). Different loading positions were employed to study the effects of the mode mixity on the loads at the crack onset. The computational results are also used to correlate and to explain the trends of the experimental data. The computational results for stress, stress intensity factor and energy release rate solutions for cracked and V-notched specimens based on the MA analysis are compared with those based on the traditional FE analyses in order to benchmark the results obtained from the MA analysis. A two-fold criterion developed by Leguillon (2002) for the crack initiation at a V-notch in specimens made of homogeneous brittle material that requires a simultaneous satisfaction of Griffith energy and stress conditions is extended for specimens under mixed-mode loading conditions. The extended Leguillon's criterion is then employed to estimate the loads at the crack initiation for the V-notch specimens of PC and PMMA. The estimated loads are rather closed to the experimental data. Finally, an inverse approach is also developed to estimate the fracture energy per unit surface, called as *fracture toughness* in this investigation, at different mode mixity ratios to study the dependence of the fracture toughness of the adhesive bonding on the mode mixity ratio.

2 Materials and experimental procedures

In order to study the influence of a bonded interface on a sharp notch, specimens as shown in Fig. 1 were tested in three-point bending and the crack initiation load was recorded. In this section, material properties of the constituents and details of experimental methods are discussed. Polycarbonate and PMMA (Piedmont Plastics, TN) were chosen as materials to make V-notched specimens as shown in Fig. 1. Each specimen is made of two individual parts which are bonded together using an adhesive to form a sharp notch compared to a machined notch (Dunn et al. 1997a). Loctite 384 (Henkel Corp., Rocky Hill, CT), a type of tough acrylic, was used as the interfacial adhesive. This adhesive was chosen such that its elastic properties are close to those of the bulk polymer. Thereby, the interface can be modeled as a line without any thickness but with different bonding strengths and fracture toughnesses (Xu et al. 2004b). Material properties of the various combinations of bonded interfaces are provided in Krishnan and Xu (2011a). The specimens were bonded together

Fig. 1 Middle Schematic plot of a V-notch specimen of two identical sheets under three-point bending conditions. Right A close up view of the notch root and the short crack along the interface. Left For clarity, Cartesian and polar coordinate systems were plotted beside the figure

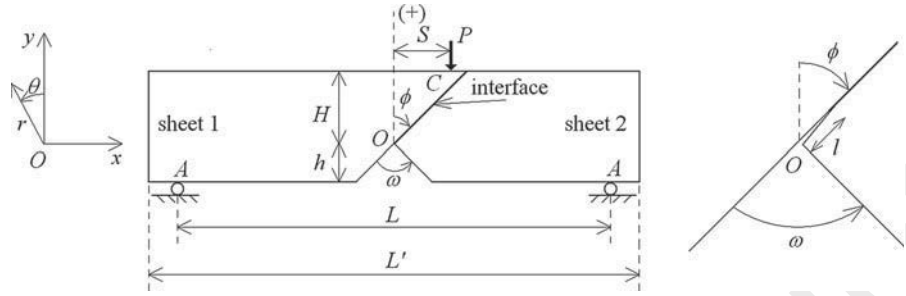


Table 1 The tensile strength σ_c , shear strength τ_c , mode I fracture toughness G_{Ic} and mode II fracture toughness G_{IIc} for PC/384/PC and PMMA/384/PMMA specimens reported in Krishnan and Xu (2011a, 2012)

	Tensile strength σ_c (MPa)	Shear strength τ_c (MPa)	Mode I fracture toughness G_{Ic} (J/m ²)	Mode II fracture toughness G_{IIc} (J/m ²)
PC/384/PC	6.06	10.99	171	325.6
PMMA/384/PMMA	12.66	11.58	140	330

using a fixture and were cured for a period of 24 hours. The method of assembly allows for the formation of a sharp notch as the excess adhesive at the notch tip was removed after bonding and prior to curing. The choice of a photoelastic polymer (polycarbonate) allows for in-situ fringe patterns to be observed and also facilitates experimental determination of crack initiation loads at the notch tip. Each specimen had the following dimensions: total length (L') of 254 mm, width ($H + h$ in Fig. 1) of 50.8 mm and thickness (b) of 5.4 mm. The height of the notch tip (h) in every specimen was fixed at 19.05 mm from the bottom in order to allow for a fair comparison between specimens of varying notch angles. In this study, three different notch angles (ω) of 30°, 90° and 120° were chosen. All the specimens have the same loading length L , measured as the distance between two roller supports, of 90 mm as shown in Fig. 1. The discrepancy between the total length and the distance between rollers is due to ignorance of the crack initiation load that might have required a greater span. For the sake of notation convenience polycarbonate (Young's modulus of 2.4 GPa and Poisson's ratio of 0.34) will be denoted as PC and Poly Methyl Methacrylate (Young's modulus of 3.6 GPa and Poisson's ratio of 0.37) will be herein denoted as PMMA (data are supplied by the manufacturers). Also, V-notch specimens of PC and PMMA bonded with Loctite-384 will be systematically denoted as PC/384/PC and PMMA/384/PMMA respectively.

All the specimens were tested in three-point bending using a standard fixture mounted on an MTS

810 machine with a crosshead displacement rate of 1 mm/min. The experimental set-up consists of three parts including a mechanical system to load the specimen, an optical system to develop fringe patterns and an imaging system to record the fringe patterns (further details in Krishnan and Xu 2012). The loading position where the vertical displacement applied is marked as S in Fig. 1. It should be noted that S is measured from the center line of the specimen and is assigned a positive value in the right-ward direction. In this investigation, the specimens were tested at three loading positions of $S = -30$ mm, $S = 0$ mm and $S = +30$ mm to investigate effects of the mode mixity ratio on the loads at the crack onset. The crack initiation load is recorded either from the load-displacement curve or by observation from the in-situ optical techniques. The latter are employed only for large angles for which the load drop is not visible enough on the load-displacement curve.

Table 1 lists the tensile strength σ_c , shear strength τ_c , mode I fracture toughness G_{Ic} and mode II fracture toughness G_{IIc} for the same PC/384/PC and PMMA/384/PMMA material systems as reported in Krishnan and Xu (2011a, 2012). For the same type of adhesive bonding, the tensile strength, the shear strength and the mode II fracture toughness for PMMA specimens are higher than PC specimens. However, the mode I fracture toughness for PMMA specimens is lower than that of PC specimens. The strength and fracture toughness of the adhesive bonding should not be considered as "material properties" since they depend

upon the combination of the bonded materials (Krishnan and Xu 2011a).

3 Experimental results

This section reports the results obtained from experimental testing. Figure 2a shows a typical load-displacement curve for a PC/384/PC specimen with a notch angle of $\omega = 90^\circ$ and loading position of $S = 0$ mm. As expected, the load increases linearly prior to the crack initiation indicated by a sharp drop in the load. For other specimens with different notch angles or bonding, if there is no clear drop in the load-displacement, in situ fringe patterns are used to detect the crack initiation. These two kinds of load drop phenomena have also been observed in Xu and Tippur (1995), Araki et al. (2005), Caimmi and Pavan (2009) for bonded similar and dissimilar material specimens. In all our specimens, crack initiation always starts from the notch tip and along the interface. After the crack initiates, there is a significant load drop as seen in Fig. 2a. The load then increases slightly prior to a second drop. This is due to high compressive force acting ahead of the crack tip, which is very close to the upper loading point. Figure 2b shows a partially failed PC/384/PC specimen with $\omega = 90^\circ$ during the three-point bending test at the loading position of $S = 0$ mm. In Fig. 2b, the bold arrow represents the vertical load induced by the applied vertical displacement u_y via a marked load roller on the top surface of the specimen. The two support rollers used to hold the specimen during three-point bending test are also shown in the figure. The V-notch specimen mainly failed by crack that initiated from the notch tip and propagated along the interface due to the fact that the strength/fracture toughness of the adhesive interface are lower than those of the bulk polymer material. The picture shows that the displacement is quite high, but the specimen has still not failed completely due to the effect of high compressive force before the crack, i.e., increased crack resistance. A detailed study of fracture surfaces will be discussed later.

This paper deals only with the crack initiation at the V-notch, rather than crack propagation along the interface. In this investigation, the experimental load at the crack initiation is denoted as F_i and the corresponding experimental stiffness of the linear portion of the load-displacement curve is denoted as S_{exp} . Table 2a, b list the values of the load at the

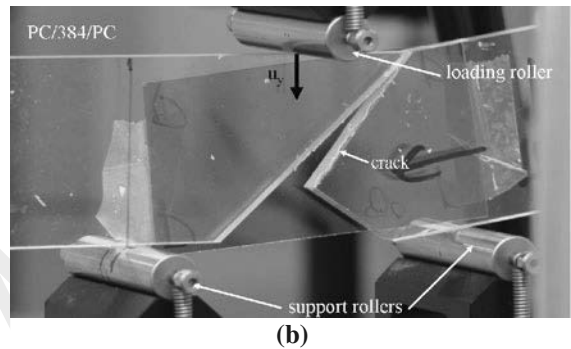
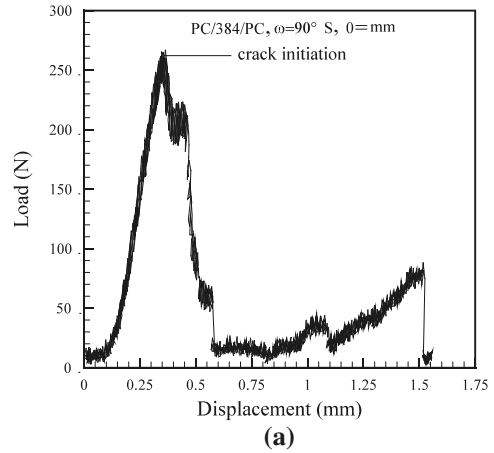


Fig. 2 a A typical load-displacement curve for a PC/384/PC specimen with a notch angle of $\omega = 90^\circ$ at the loading position of $S = 0$ mm, b a failed PC/384/PC specimen with $\omega = 90^\circ$ during the three-point bending test at the loading position of $S = 0$ mm

crack initiation F_i and the experimental stiffness S_{exp} for PC/384/PC and PMMA/384/PMMA specimens, respectively, under different loading positions S . At least three identical V-notch specimens were tested for each loading condition. Some lacking data as listed in Table 2a, b are due to the abnormally weak bonded specimens and data missing. The use of computational results to explain the trends of the data will be reported in the next sections.

4 Leguillon's criterion for crack initiation at a V-notch

As mentioned earlier, the V-notch specimens failed due to a crack initiating at the tip and propagating along the interface. In order to predict the load at the crack initiation, the two-fold Leguillon's criterion for the crack initiation at a V-notch in the homogenous specimen

Table 2 The values of the load at the crack onset F_i and the experimental stiffness S_{exp} for (a) PC/384/PC, (b) PMMA/384/PMMA specimens under different loading positions S

Notch Angle	$S = -30 \text{ mm}$		$S = 0 \text{ mm}$		$S = 30 \text{ mm}$	
	$F_i \text{ (N)}$	$S_{\text{exp}} \text{ (N/mm)}$	$F_i \text{ (N)}$	$S_{\text{exp}} \text{ (N/mm)}$	$F_i \text{ (N)}$	$S_{\text{exp}} \text{ (N/mm)}$
(a) For PC/384/PC specimens						
30°	535.5	1866.5	221.7	1449	392.5	1638.5
90°	1051	1849.3	329	1194	477	1691.7
120°	1100	-	378	1224	906.3	1920.7
(b) For PMMA/384/PMMA specimens						
30°	666.3	2300	276.7	1550.3	522	2369
90°	1341	2428	351.7	1754.3	747	2104
120°	1498	2288.3	454.7	1593.3	940.7	2485.7

will be employed. The criterion for a crack initiation at a V-notch specimen developed by Leguillon (2002) is summarized in this section.

4.1 Singularity at a V-notch

Cartesian (x, y) and polar (r, θ) coordinates are shown in Fig. 1. The two sheets are assumed to be isotropic and linear elastic with the Young's modulus E and Poisson's ratio ν . They are also assumed to be perfectly bonded along the interface. The notch tip is located at point O as shown in the figure and ω denotes the notch angle. The interface between the two sheets makes an angle $\phi = \omega/2$ with the bisector.

Within the framework of linear elasticity and the assumption of plane strain condition (which is always preferable for fracture mechanics models), the displacement field and the corresponding stress field in the vicinity of the singular point O (the notch tip) can be expressed in an asymptotic expansions as (Williams 1952)

$$\begin{cases} \underline{U}(r, \theta) = \underline{R} + k_1 r^{\lambda_1} \underline{u}_1(\theta) + k_2 r^{\lambda_2} \underline{u}_2(\theta) + \dots \\ \quad = \underline{R} + k_1 r^{\lambda_1} [\underline{u}_1(\theta) + m(r) \underline{u}_2(\theta)] + \dots \\ \underline{\sigma}(r, \theta) = k_1 r^{\lambda_1 - 1} \underline{s}_1(\theta) + k_2 r^{\lambda_2 - 1} \underline{s}_2(\theta) + \dots \\ \quad = k_1 r^{\lambda_1 - 1} [\underline{s}_1(\theta) + m(r) \underline{s}_2(\theta)] + \dots \\ \text{with } m = \frac{k_2}{k_1} r^{\lambda_2 - \lambda_1} \end{cases} \quad (1)$$

For the case of a single singular eigenvalue (i.e. for wide openings $\omega \geq 105^\circ$), Eq. (1) holds with $m(r) = 0$. Vector \underline{R} is a rigid-body translation, λ_i ($i = 1, 2$) represent eigenvalues associated with the displacement and stress angular eigenfunctions $\underline{u}_i(\theta)$ and $\underline{s}_i(\theta)$, respectively. The parameters k_i , so-called generalized stress intensity factors (GSIF), are proportional to the applied load. Note that the eigenvalue λ_i must

be positive for a finite energy solution. Note also that only leading eigenvalues $\lambda_i < 1$ are of our interests since the corresponding stress fields tend to infinity as $r \rightarrow 0$, i.e., when approaching the notch tip. There is a stress concentration around this point. For the V-notch of two sheets made of a similar material, the singular eigenvalues are real, single or multiple (Williams 1952; Leguillon and Sanchez-Palencia 1987; Vu-Quoc and Tran 2005), whereas in bimetals or more complex geometries, there is no fixed rule to decide if the exponents are real or complex.

Note that parameter $m(r)$ depends on the distance r ahead the notch tip except in case of a double root $\lambda_1 = \lambda_2$. The parameter $m(r)$ does not represent the physical mode mixity ratio as discussed later, it has a pure mathematical definition. It should be also emphasized that for the case of $\omega = 0$ (a crack), the two eigenmodes shown in Eq. (1) merge with the two conventional mode I and mode II.

The extraction of the generalized intensity factors from the elastic solution can be carried out based on a path independent integral Ψ computed on any arbitrary contour C starting and ending on the free edges of the V-notch (Leguillon and Sanchez-Palencia 1987; Labossiere and Dunn 1999; Vu-Quoc and Tran 2005)

$$\Psi(\underline{U}, \underline{V}) = \frac{1}{2} \int_C [\underline{\sigma}(\underline{U}) \cdot \underline{n} \cdot \underline{V} - \underline{\sigma}(\underline{V}) \cdot \underline{n} \cdot \underline{U} ds] \quad (2)$$

for all functions \underline{U} and \underline{V} in equilibrium. Here, C is an arbitrary contour encircling the singular point, and \underline{n} is its normal pointing toward the singular point. For the case of a single eigenvalue λ_i , the generalized stress intensity factor k_i in Eq. (1) is obtained as

$$k_i = \frac{\Psi(\underline{U}^{\text{FE}}(r, \theta), r^{-\lambda_i} \underline{u}_i^-(\theta))}{\Psi(r^{\lambda_i} \underline{u}_i(\theta), r^{-\lambda_i} \underline{u}_i^-(\theta))} \quad (3)$$

where $r^{-\lambda_i} \underline{u}_i^-(\theta)$ denotes the mode that is dual to the mode $r^{\lambda_i} \underline{u}_i(\theta)$ (see Leguillon and Sanchez-Palencia (1987) for details on the existence and the role of these solutions) and where $\underline{U}^{\text{FE}}(r, \theta)$ is the FE approximation of the exact elastic solution of the displacement field. Note that both modes (primary and dual) are obtained analytically or numerically. This method can be extended to the cases of two real eigenvalues and even to complex eigenvalues (Leguillon and Sanchez-Palencia 1987).

4.2 The two-fold Leguillon's criterion for the crack initiation at a V-notch

As discussed in Leguillon (2002), due to the crack initiation at the notch tip with a crack length l along the interface (i.e. making an angle ϕ with the bisector), under fixed loading conditions, the potential energy of the specimen has changed. The change in potential energy $-\delta W_p(l)$ is defined as the difference of the potential energy of the initially unperturbed state and that of the perturbed state (i.e. embedding the short crack l , Fig. 1). For the case of two eigenvalues as shown in Eq. (1), $-\delta W_p$ can be written as

$$-\delta W_p(l) = k_1^2 l^{2\lambda_1} \times \left(A_{11}(\phi) + 2m(l)A_{12}(\phi) + m(l)^2 A_{22}(\phi) \right) + \dots \quad (4)$$

where the scaling coefficients A_{11} , A_{12} and A_{22} depend on ϕ and are obtained from a MA procedure (Leguillon 2002; Leguillon and Siruguet 2002; Yosibash et al. 2006).

- (i) First, the energy condition requires an energy balance between the initial unperturbed state and the perturbed state

$$\delta W_p(l) + \delta W_k(l) + G_c \delta S = 0 \quad (5)$$

Here, $\delta W_p(l)$ and $\delta W_k(l)$ are the changes in potential and kinetic energies, respectively. The newly created crack surface is denoted $\delta S = l \cdot b$ (b is the specimen thickness) and G_c is the fracture toughness, i.e., the fracture energy per unit surface.

Since $\delta W_k(l) \geq 0$ in quasi-static conditions, a necessary condition for fracture is

$$-\frac{\delta W_p(l)}{\delta S} = G^{\text{inc}} \geq G_c \quad (6)$$

Equation (6) is an incremental form of the energy criterion as it requires the knowledge of the parameter δS . It is the foundation of the Finite Fracture Mechanics (Hashin 1996; Taylor et al. 2005). Note that, usually the limit $\delta S \rightarrow 0$ is considered and leads to the classical Griffith criterion (differential form of the energy criterion).

- (ii) Second, the stress condition requires that

$$\begin{aligned} \sigma_{\theta\theta}(r, \phi) &\geq \sigma_c \quad \text{for } 0 \leq r \leq l \Rightarrow \sigma_{\theta\theta}(l, \phi) \\ &\simeq k_1 l^{\lambda_1 - 1} (s_{1\theta\theta}(\phi) + m(l)s_{2\theta\theta}(\phi)) \geq \sigma_c \end{aligned} \quad (7)$$

$\sigma_{\theta\theta}(r, \phi)$ is the hoop stress at the distance r of the notch root along the interface and σ_c is the tensile strength of the material or the interface.

It is postulated by Leguillon (2002) that both energy and stress conditions are necessary for initial cracking but neither one nor the other is sufficient. As discussed in detail in Leguillon (2002) in case of a single eigenvalue and in Yosibash et al. (2006) in case of two eigenvalues for homogeneous material notched specimens, a consequence of the energy balance is that, at initiation, the crack jumps a length l_c and the consistency between the two conditions (i) and (ii) leads to the Irwin-like condition

$$\begin{aligned} k_1 \geq k_c &= \left(\frac{G_c}{A_{11} + 2m_c A_{12} + m_c^2 A_{22}} \right)^{1-\lambda_1} \\ &\times \left(\frac{\sigma_c}{s_{1\theta\theta} + m_c s_{2\theta\theta}} \right)^{2\lambda_1 - 1} \end{aligned} \quad (8)$$

where

$$\begin{aligned} m_c &= m(l_c) = \frac{k_2}{k_1} l_c^{\lambda_2 - \lambda_1} \quad \text{and} \\ l_c &= \frac{G_c}{A_{11} + 2m_c A_{12} + m_c^2 A_{22}} \left(\frac{s_{1\theta\theta} + m_c s_{2\theta\theta}}{\sigma_c} \right)^2 \end{aligned} \quad (9)$$

For simplicity, the dependence on ϕ occurring through the A_i and $s_{i\theta\theta}$ is no longer explicitly written.

Leguillon's criterion (Eq. (8)) has been validated by experiments of V-notched homogeneous specimens of PMMA and ceramics sheets under symmetric static loading conditions (Seweryn 1994; Dunn et al. 1997a; Leguillon 2002; Leguillon and Yosibash 2003b). According to these authors, the critical value k_c must be experimentally determined for each value of

the singular eigenvalue λ_1 , i.e. for each notch angle ω , since the factors k_1 and k_c are strongly dependent on the notch angle. Comparison with experiments under non symmetric loading conditions was proposed in Yosi-bash et al. (2006) and Leguillon et al. (2009).

As shown in Eq. (8), when λ_1 tends to 0.5, the crack initiation at the V-notch is dominantly due to the satisfaction of the energy criterion since the exponent $(2\lambda_1 - 1)$ of σ_c tends to 0. In contrast, when λ_1 tends to 1, i.e. for large openings, the crack initiation at the V-notch is dominantly due to the satisfaction of the stress criterion since the exponent $(1 - \lambda_1)$ of G_c tends to 0. As listed in Table 4, the values of λ_1 are quite close to 0.5 for the V-notch specimens tested in this investigation. This remark appears to be useful in the design of notch angles for the tests of specimens made of similar or different sheet materials.

In this investigation, we will first extend Leguillon's criterion in Eq. (8) by considering the stress and energy conditions under mixed-mode loading conditions. Then, the extended Leguillon's criterion is employed to estimate the loads at the crack initiation for V-notch specimens joint by an adhesive bonding.

5 Correlation of computational and experimental results

5.1 Comparison of computational results based on MA and FE analyses

In order to benchmark the computational results obtained from the MA analysis presented in the previous section, the computational results based on the MA analysis are compared with those based on the traditional FE analysis. It should be noted that for a special case of $\omega = 0$ (a cracked specimen), the generalized stress intensity factor solutions k_1 and k_2 defined in Eq. (1) become the conventional stress intensity factor solutions K_I and K_{II} , respectively. In reference to Fig. 1 with $\omega = 0^\circ$ and $S = 0$ mm, the mode I stress intensity factor solution K_I can be estimated as (Anderson 2004)

$$K_I = \frac{PL}{B(h+H)^{3/2}} f(x) \quad (10)$$

with

$$x = \frac{h}{h+H} \quad (11)$$

and

$$f(x) = \frac{3}{2} \sqrt{x} \frac{[1.99 - x(1-x)(2.15 - 3.93x + 2.7x^2)]}{(1+2x)(1-x)^{3/2}} \quad (12)$$

The values of K_I based on Eqs. (10–12) and the same applied load are listed in Table 3 and compared to the stress intensity factor K_I and K_{II} obtained from the MA and FE analyses. As listed in the table, the computational results based on the MA and FE analyses agree well with the available analytical solutions. Note that one of the benefits of the path independent integral Ψ is that the stress intensity factors K_I and K_{II} can be computed directly without a need to perform the interaction integral method to separate the two modes as in ABAQUS (2004).

To verify the solutions obtained from the MA analysis, FE analyses are conducted to obtain the stress and energy release rate solutions. It should be noted that the actual adhesive interface is not modeled in the computational analyses in this investigation due to the fact that its thickness (at the order of few microns) is very small as compared with the other geometric parameters of the specimen, moreover the Young's moduli of the adhesive and the polymer are very close to each other. It is simply a support line of the mesh, a so-called "fictitious bond line". However, the indication of the adhesive is kept in the specimen names when discussing the computational results for consistent presentation.

Figure 3a shows the computational results for stress $\sigma_{\theta\theta}$ and energy release rate G solutions as functions of the distance from the notch along the bond line based on the MA and traditional FE analyses for a PC/384/PC specimen with $\omega = 90^\circ$ at the loading position of $S = 0$. Figure 3b shows a close-up view of Fig. 3a near the notch tip. Note that the results for $\sigma_{\theta\theta}$ are obtained

Table 3 Stress intensity factors K_I and K_{II} obtained from the MA and the analytical solutions

	Loading position $S = 0$ mm	Loading position $S = 30$ mm
From the MA analysis	$K_I = 94.3\text{MPa}\sqrt{\text{mm}}$	$K_I = 98.9\text{MPa}\sqrt{\text{mm}}$ $K_{II} = 12.1\text{MPa}\sqrt{\text{mm}}$
Analytical solutions (Anderson, 2004)	$K_I = 96.2\text{MPa}\sqrt{\text{mm}}$	

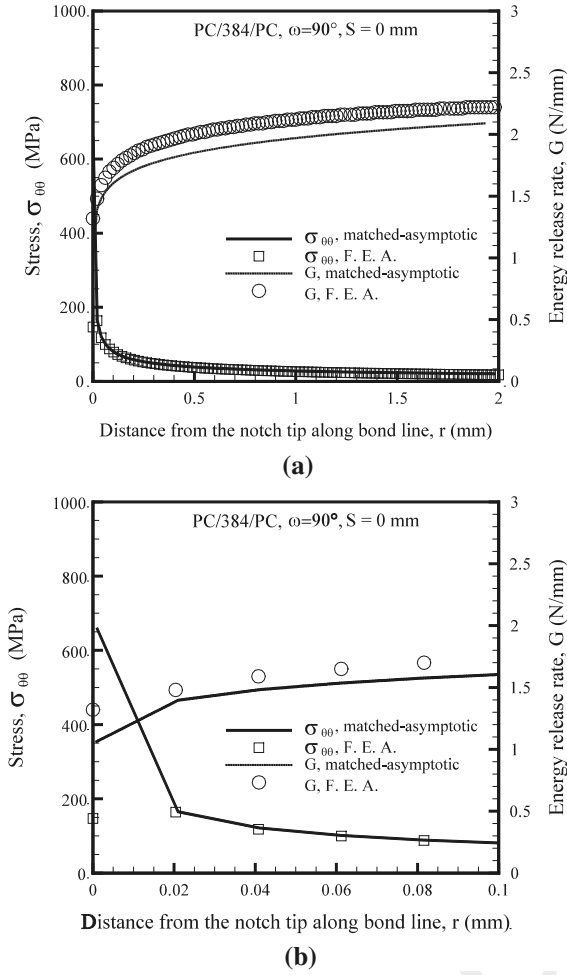


Fig. 3 a computational results for stress $\sigma_{\theta\theta}$ and energy release rate G as functions of the distance to the notch along the bond line based on the MA and FE analyses for a PC/384/PC specimen with $\omega = 90^\circ$ at the loading position of $S = 0$, b a close-up view of (a) near the notch tip

from the V-notch specimen without a crack. For the calculation of the energy release rate $G(l)$, the nodes from the notch tip along the “fictitious bond line” are unbuttoned node by node to create cracks with different lengths along the bond line. Then, for each crack length l , $G(l)$ is approximated by

$$G(l) \approx -\frac{W_p(l + \Delta l) - W_p(l)}{\Delta l} \quad (13)$$

where l denotes the current crack length along the bond line, Δl represents the step of crack advancement and W_p represents the potential energy.

In this investigation, a uniform step of $\Delta l = 20 \mu\text{m}$ is used to calculate the energy release rates within a

distance of 2 mm from the notch tip along the bond line. For the FE models without and with cracks, in reference to Fig. 1, the displacement boundary conditions with $u_y^A = 0$ and $u_y^C = -1 \text{ mm}$ are employed. As shown in Fig. 3a, b, the computational results based on the MA analysis agree well with those based on the FE analysis within a range from 0.02 to 2 mm from the notch tip. When approaching the corner, the stress solution based on the MA analysis is larger than that based on the FE analysis since the singularity is not considered in the FE analysis and a kind of truncation occurs. This range from 0.02 to 2 mm from the notch tip represents a zone where the stress solution is scaled by the leading terms in Williams’ asymptotic analysis. This zone may be perceived as a “ k -dominance zone” for a V-notch as an analogue to the K -dominance zone for a crack as widely accepted in the conventional fracture mechanics. For other specimens with different notch angles tested at different loading positions S , the computational results based on the MA analysis also agree well with those based on the FE analysis within a range from tens of microns to about 2 mm from the notch tip. For crack lengths larger than 2 mm, the solutions based on the MA analysis cease to agree satisfactorily with those based on the FE analysis due to the fact that the displacement and stress solutions in Eq. (1) based on the MA analysis are accurate only within a zone close to the notch tip. The comparison of the computational results in Table 3 and Fig. 3 suggests that the MA analysis presented in this investigation can be used to obtain the energy release rate solutions for short cracks initiated from a V-notch without a need to perform very fine meshes as required in traditionally FE analysis. Recently, Leguillon (2011) proposed a method to determine the length of a short crack at a V-notch from a full field measurement also based on the MA analysis.

5.2 Mode mixity ratio

It should be noted that the fracture toughness of the adhesive bonding between two identical or dissimilar sheet materials appears to strongly depend on the mode mixity near the crack tip (Suo and Hutchinson 1990; Xu and Tippur 1995; Xu et al. 2003; Araki et al. 2005; Caimmi and Pavan 2009). Note that for a crack, mode I and mode II loading conditions correspond to an “opening mode” and a “sliding mode” of crack faces, respectively. However, a definition of the “opening mode”

and “sliding mode” is not obvious in the present case for an inclined crack corresponding to a V-notch with $\omega > 0$. Here, the mode mixity ratio $\psi(r, \theta)$ is defined as the ratio of the shear stress $\sigma_{r\theta}$ to the normal stress $\sigma_{\theta\theta}$ measured at a distance $r = l_0$ ahead the notch tip along the line $\theta = \text{constant}$ of a V-notch as

$$\psi(\theta) = \left. \frac{\sigma_{r\theta}(\theta)}{\sigma_{\theta\theta}(\theta)} \right|_{r=l_0} \quad (14)$$

As discussed earlier, within a small distance from the notch tip, the stress solutions computed from the conventional FE analysis are nearly identical to those obtained from Eq. (1) based on the MA analysis. Therefore, $\psi(r, \theta)$ can be obtained from the MA analysis as

$$\begin{aligned} \psi(r, \theta) &= \frac{k_1 r^{\lambda_1 - 1} s_{1r\theta}(\theta) + k_2 r^{\lambda_2 - 1} s_{2r\theta}(\theta)}{k_1 r^{\lambda_1 - 1} s_{1\theta\theta}(\theta) + k_2 r^{\lambda_2 - 1} s_{2\theta\theta}(\theta)} \\ &= \frac{s_{1r\theta}(\theta) + m(r) s_{2r\theta}(\theta)}{s_{1\theta\theta}(\theta) + m(r) s_{2\theta\theta}(\theta)} \end{aligned} \quad (15)$$

where $m(r)$, $s_{kr\theta}(\theta)$ and $s_{k\theta\theta}(\theta)$ ($k = 1, 2$) are defined in Eq. (1). Dependence of the mode mixity ratio on the radius may be surprising but it is also found in Hutchinson and Suo (1992) in a slightly different form. This is unavoidable and inherent in the presence of distinct exponents (the complex exponent and its conjugate in the case of the interface cracks presented by Hutchinson and Suo 1992).

Figure 4 shows the mode mixity ratio ψ as functions of the distance r along the bond line $\theta = \phi$ from the notch tip for a PC/384/PC specimen with $\omega = 90^\circ$ at different loading position S . Note that the mode mixity ratios ψ shown in Fig. 4 are obtained from Eq. (14). As shown in the figure, for a fixed distance r , the mode mixity ratio ψ increases when the loading position S increases. As shown in Fig. 4, the values of mode mixity ratio ψ are nearly the same in the vicinity of the notch tip for all three loading positions S . From Eq. (15), when the distance r tends to 0 (at the notch tip), then $\psi(r \rightarrow 0)$ tends to $s_{1r\theta}(\theta)/s_{1\theta\theta}(\theta)$ which do not depend on the loading position as confirmed by Fig. 4. The mode mixity ratio ψ varies slowly for a distance r from 0.05 to 2 mm. The characteristic length l_0 should be selected within “ k -dominance zone” for a V-notch as defined earlier, it has also to agree with a recommendation of Rice (1988) for an interface crack. Therefore, in this investigation, the values of the mode mixity ratio ψ are evaluated at a distance of $l_0 = 0.5$ mm from the notch tip along the bond line. The trends of ψ for PC/384/PC specimens with the notch

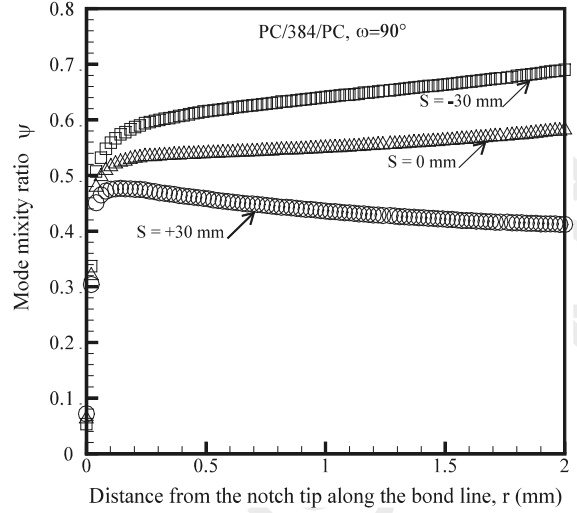


Fig. 4 The mode mixity ratio ψ as functions of the distance r along the bond line from the notch tip for a PC/384/PC specimen with $\omega = 90^\circ$ at different loading positions S

angles of $\omega = 30^\circ$ and $\omega = 120^\circ$ are similar to those shown in Fig. 4 and are not reported here. Note also that for a V-notch of two identical sheets, ψ does not depend on the Young’s modulus of the sheet material. The values of ψ for the PMMA/384/PMMA specimens are therefore the same as those for the PC/384/PC specimens with the same notch angle.

5.3 Correlation of computational and experimental results

Table 4 lists the computational results for PC/384/PC specimens based on the MA analysis. These computational results will be used later to estimate the loads at the crack onset. Note that the results listed in Table 4a do not depend on the loading position S . Note also that for the V-notch specimens made of two identical sheets, $\lambda_1, \lambda_2, s_{1r\theta}, s_{1\theta\theta}, s_{2r\theta}$ and $s_{2\theta\theta}$ do not depend on the Young’s modulus of the sheet material and A_{11}, A_{12} and A_{22} are inversely proportional to the Young’s modulus. Results are listed in Table 4a, b.

It should be pointed out that the computational results listed in Table 4b are obtained when the boundary conditions of $u_y^A = 0$ and $u_y^C = -1$ mm are employed. It is then easy to derive the effective computational specimen stiffness, denoted as S_{comp} in Table 4b. For convenient discussion, the mean values of the experimental load at the crack initiation F_i and

Table 4 Computational results for PC/384/PC specimens based on the MA analyses when a displacement of 1 mm is applied at the corresponding loading positions

(a) MA analysis parameters									
ω (°)	λ_1	λ_2	$s_{r\theta}^{(1)}$	$s_{\theta\theta}^{(1)}$	$s_{r\theta}^{(2)}$	$s_{\theta\theta}^{(2)}$	A_{11} MPa ⁻¹	A_{12} MPa ⁻¹	A_{22} MPa ⁻¹
30	0.5015	0.5981	-13	90	-64	27	34.7	0.42	14.4
90	0.5446	0.9075	-58	108	-8	33	7.2	0.26	7.7
120	0.6158	1.1490	99	103	-21	66	-16.31	0.17	-16.42
(b) Theoretical results and experiments									
Notch angle ω (deg)	Loading position S (mm)	GSIF k_1 MPa mm ^{1-λ_1}	GSIF k_2 MPa mm ^{1-λ_2}	Mode mixity ψ	Effective stiffness S_{comp} (N/mm)	Exp. Load at crack onset F_i (N)	Exp. stiffness S_{exp} (N/mm)		
30	-30	0.4325	-0.0638	0.261	1060.4	535.5	1866.5		
	0	0.4170	0	0.141	709.5	222	1449		
	+30	0.4244	0.0638	0.028	1060.4	393	1638.5		
90	-30	0.26	-0.102	0.615	1034	968	1849.3		
	0	0.263	0	0.539	704	329	1194		
	+30	0.2592	0.108	0.459	1012	477	1691.7		
120	-30	0.164	0.0347	1.01	968	1100	1854.3		
	0	0.1698	0	0.953	671	378	1224		
	+30	0.1632	-0.0347	0.894	968	906	1920.7		

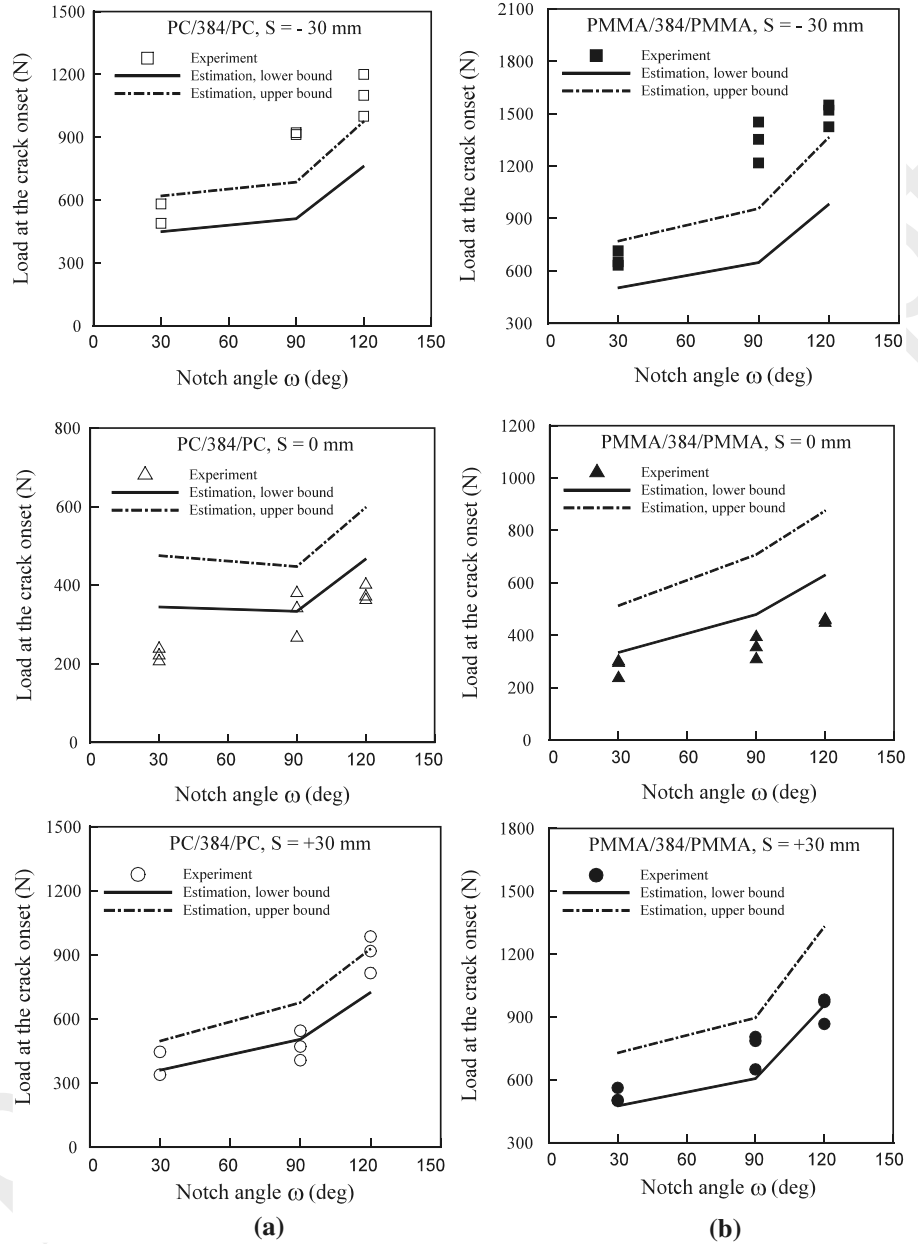
the experimental stiffness S_{exp} listed in Table 2 are also included in Table 4b. Instead of mean values, a detailed presentation can be found in Krishnan and Xu (2012). However one can get an idea of the scattering in Figs. 5 and 6. The computational parameters for the PMMA/384/PMMA specimens can be easily obtained from the data listed in Table 4a, b for the PC/384/PC specimens.

As listed in Table 4a, b, for a fixed loading position S , the eigenvalues λ_1, λ_2 and the mode mixity ratio ψ increase when the notch angle ω increases. Also, the effective computational specimen stiffness S_{comp} slightly decreases when the notch angle ω increases, possibly due to the fact the V-notch specimen with a larger notch angle has a bit less sheet material. Note that the stress solution is less singular at a larger eigenvalue λ_1 and that the fracture toughness G_c of the adhesive bonding is in general higher at the larger mode mixity ratio ψ . These remarks can partially explain why the experimental load at the crack initiation F_i increases when the notch angle ω increases. It should also be noted that the units of k_1 (MPa mm^{1- λ_1}) differ from one value of λ_1 to another and thus any direct comparison between the two values of k_1 for specimens of two different notch angles is strictly impossible.

As listed in Table 4b, for a fixed notch angle ω , the generalized stress intensity factor k_1 first slightly

decreases and then slightly increases when the loading position S increases from -30 mm to +30 mm. The computed values of k_1 for $S = -30$ mm are slightly different from those for $S = +30$ mm because the density of the FE mesh is not totally symmetric with respect to the vertical line of the specimen since the two sheets are meshed separately with respect to the “fictitious bond line”. Note that the mesh densities used in the FE analyses are carefully chosen to minimize the mesh-sensitivity. When the offset of the loading position S increases, the absolute value of k_2 and the effective specimen stiffness S_{comp} first decrease and then increase while the mode mixity ratio ψ monotonically decreases. Note also that for the same applied displacement, a higher load is needed to fracture the specimen with a higher effective stiffness S_{comp} . By using the same observations on the effects of ψ and S_{comp} on the load at the crack initiation as discussed earlier, one can partially explain why the experimental load at the crack initiation F_i first decreases and then increases when the loading position S moves from -30 to 30 mm. Note that the values of S_{comp} and k_1 are nearly the same for the cases of $S = -30$ mm and $S = +30$ mm since the adhesive bonding that causes the asymmetry is not modeled in the computations. The larger values of F_i for the loading position of $S = -30$ mm as compared to those for the loading position $S = +30$ mm

Fig. 5 Upper and lower bounds of the load estimation for **a** PC/384/PC, **b** PMMA/384/PMMA specimens by using the extended Leguillon's criterion in Eq. (20)



may be due to the larger values of the mode mixity ratio ψ .

As shown in Table 4b, for each loading position, the values of S_{comp} are about 50–65 % of those of S_{exp} for the PC/384/PC specimens. Also, in reference to Fig. 1, it is noteworthy that a free displacement in the horizontal direction is applied at the two roller supports for the computations ($u_y^A = 0$). In fact, the horizontal displacement at the roller supports may not be totally free due to the contact and the friction between the

rollers and the specimen during the test. This remark may explain why with this prescribed boundary condition, the computational stiffness is smaller than the experimental stiffness. Other FE analyses in which both horizontal and vertical displacements at the two roller supports was restraint ($u_y^A = u_x^A = 0$) are also performed. The computational results show that the values of S_{comp} obtained from the FE analysis with the boundary condition of $u_y^A = u_x^A = 0$ are now higher than the experimental stiffness. The actual situation lies

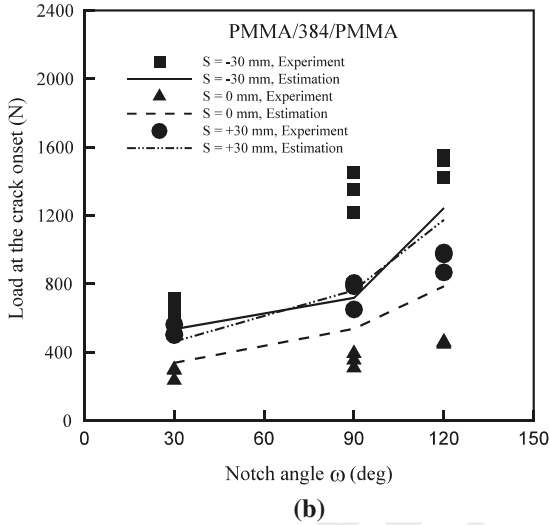
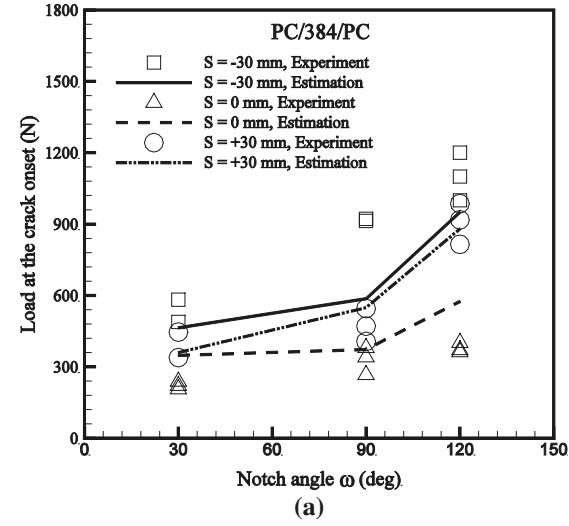


Fig. 6 Estimated loads at the crack initiation for PC/384/PC and PMMA/384/PMMA specimens by using the extended Leguillon's criterion in Eq. (27)

somewhere between these two bounds. The use of one or the other boundary condition actually under or over-estimates the experimental stiffness. Therefore, the difference in the values of S_{comp} and S_{exp} may be due to the fact that the physical boundary conditions during the three-point bending test were not accurately modeled in the computations.

6 Extension of Leguillon's criterion to mixed-mode crack initiation

It should be emphasized that only simple and generic stress and energy conditions were shown in Eq. (8).

In this investigation, the crack initiation at the V-notch tip along the interface is under general mixed-mode loading conditions. Therefore, different stress and energy conditions under mixed-mode loading conditions are used to extend Leguillon's criterion which is then used to estimate the loads at the crack initiation for PC/384/PC and PMMA/384/PMMA V-notch specimens.

6.1 Stress and energy conditions under mixed-mode loading conditions

The extended Leguillon's criterion can be rewritten under a general form as

$$k_1(F) \geq k_c = f(\sigma_c, \tau_c, G_{Ic}, G_{IIc}) \quad (16)$$

where G_{Ic} and G_{IIc} denote mode I and mode II toughnesses and σ_c and τ_c the tensile and shear strengths, respectively.

First, stress and energy conditions in Eq. (8) are extended, respectively, to account for the mixed-mode loading conditions as

$$\frac{G_I(l)}{G_{Ic}} + \frac{G_{II}(l)}{G_{IIc}} \geq 1 \quad (17)$$

and

$$\sqrt{\left(\frac{\sigma_{\theta\theta}(l)}{\sigma_c}\right)^2 + \left(\frac{\sigma_{r\theta}(l)}{\tau_c}\right)^2} \geq 1 \quad (18)$$

Relation (18) is a classical elliptic condition, relation (17) allows smoothly moving from G_{Ic} to G_{IIc} . Other relationships can be chosen without fundamentally changing the results, especially if σ_c and τ_c on the one hand and G_{Ic} and G_{IIc} on the other hand are not too far from each other as is the case here. Relation (17) can be replaced for instance by the Hutchinson and Suo (1992) rule (see Garcia and Leguillon 2012), G_c is defined as a function of G_{Ic} and G_{IIc} and the energy condition can be written $G_I(l) + G_{II}(l) \geq G_c$.

6.2 Upper and lower bounds for the critical failure load

It should be noted that the energy release rate G^{inc} determined from Eqs. (4) to (6) represents the total (incremental) energy release rate for a crack initiated at the V-notch tip based on the MA analysis. However,

it is impossible to decompose into the sum of two conventional mode I and mode II energy release rates G_I and G_{II} , respectively. To overcome this difficulty and for simplicity, two simplified form of (19) can be tested

$$\frac{G(l)}{G_{Ic}} \geq 1 \text{ or } \frac{G(l)}{G_{IIc}} \geq 1 \quad (19)$$

Then by using Eqs. (18) and (19), the extended Leguillon's criterion in Eq. (8) can be rewritten as

$$k_1(F) \geq k_c = \left(\frac{G_{Jc}}{A_{11} + 2m_c A_{12} + m_c^2 A_{22}} \right)^{1-\lambda_1} \times \left(\frac{\sigma_c}{\sqrt{\left(s_{\theta\theta}^{(1)} + m_c s_{\theta\theta}^{(2)} \right)^2 + \frac{\sigma_c^2}{\tau_c^2} \left(s_{r\theta}^{(1)} + m_c s_{r\theta}^{(2)} \right)^2}} \right)^{2\lambda_1-1} \quad (20)$$

$J = I, II$

where the initiation crack jump l_c is obtained by solving

$$l_c = \left(\frac{G_{Jc}}{A_{11} + 2m_c A_{12} + m_c^2 A_{22}} \right) \times \left(\frac{\left(s_{\theta\theta}^{(1)} + m_c s_{\theta\theta}^{(2)} \right)^2 + \frac{\sigma_c^2}{\tau_c^2} \left(s_{r\theta}^{(1)} + m_c s_{r\theta}^{(2)} \right)^2}{\sigma_c^2} \right) \quad J = I, II \quad (21)$$

In Eqs. (20–21), m_c , function of l_c , is defined as in Eq. (9). Since, as listed in Table 1, the value of G_{IIc} is in general larger than that of G_{Ic} , the first case, $J = I$ will provide a lower bound while $J = II$ will provide an upper one for the estimation of the loads at the crack onset.

Once k_c is known, the estimated load at the crack initiation F_{est} will be obtained from

$$F_{est} = \frac{k_c F_{rec}}{k_1} \quad (22)$$

where k_1 is the generalized stress intensity factor associated with a reaction force F_{rec} obtained from FE simulations.

Figure 5a, b show the upper and lower bounds of the load estimations for PC/384/PC and PMMA/384/PMMA specimens, respectively, by using the extended Leguillon's criteria in Eq. (20) compared to experiments. As discussed earlier, there is a difference between the values of the specimen stiffness measured from the experiment (S_{exp}) and obtained from the FE analysis (S_{comp}). Since it is very difficult to model accurately the contact and friction between the two support rollers and the specimens during three-point

bending tests, the estimated values of the load at the crack initiation obtained from Eqs. (20) and (22) by using the computational results from the FE analysis with the boundary condition of $u_y^A = 0$ will be corrected by a ratio of S_{exp}/S_{comp} . Leguillon's criterion in its extended form (Eq. (20)) appears to provide reasonably good upper and lower bounds of the estimated loads at the crack onset, the magnitudes and trends are preserved. In summary, due to lacking of further information on the dependence of the fracture toughness on the mode mixity ratio, the use of Leguillon's criterion in Eq. (20) provides a simple method to estimate the lower and upper bounds of the loads at the crack initiation along the adhesive bonding in V-notch specimens under mixed-mode loading conditions.

6.3 Estimation of loads at the crack initiation by using the mixed-mode energy condition

In an attempt to decompose the total energy release rate G based on the MA analysis for a V-notch specimen with $\omega > 0$ into the two modes I and II energy release rates G_I and G_{II} , we assume that the mode mixity ratio ψ can be approximated as

$$\tan \psi = \sqrt{\frac{G_{II}}{G_I}} \quad (23)$$

where $\tan \psi$ is obtained from Eq. (14). Then, G_I and G_{II} can be obtained as

$$G_I = \frac{1}{1 + \tan^2 \psi} G^{inc} \quad \text{and} \quad G_{II} = \frac{\tan^2 \psi}{1 + \tan^2 \psi} G^{inc} \quad (24)$$

Then the energy condition in Eq. (17) becomes

$$\frac{G^{inc}(l)}{G_c} \geq 1 \quad (25)$$

By introducing a nominal fracture toughness $\overline{G_{Ic}}$ as

$$\overline{G_c} = \frac{G_{Ic}}{\frac{1}{1 + \tan^2 \psi} + \left(\frac{\tan^2 \psi}{1 + \tan^2 \psi} \right) \frac{G_{Ic}}{G_{IIc}}} \quad (26)$$

Equations (25) and (26) were obtained thanks to assumption (17), they does not require any additional adjustable parameter like in the approach of Hutchinson and Suo (1992). The energy condition in Eq. (25) is similar to that in Eq. (19), therefore, the stress condition in Eq. (18) and the energy condition in Eq. (25) can be combined to extend Leguillon's criterion for the crack initiation under mixed-mode loading conditions as

$$k_1(F) \geq k_c = \left(\frac{\overline{G}_c}{A_{11} + 2m_c A_{12} + m_c^2 A_{22}} \right)^{1-\lambda_1} \times \left(\frac{\sigma_c}{\sqrt{(s_{\theta\theta}^{(1)} + m_c s_{\theta\theta}^{(2)})^2 + \frac{\sigma_c^2}{\tau_c^2} (s_{r\theta}^{(1)} + m_c s_{r\theta}^{(2)})^2}} \right)^{2\lambda_1-1} \quad (27)$$

where the critical initiation crack length l_c is obtained by solving an equation analogous to (21) where \overline{G}_c replaces G_{Jc} and m_c is a function of l_c defined by (9).

Figure 6a, b show the estimated loads at the crack initiation for PC/384/PC and PMMA/384/PMMA specimens, respectively, by using the extended Leguillon's criterion in Eq. (27). The correction factor of $S_{\text{exp}}/S_{\text{comp}}$ was also used in the estimation process as in the previous section. As shown in these figures, the estimated load at crack initiation for both types of specimens agree reasonably well with the experimental data for the loading positions $S = 0$ mm and $S = +30$ mm. It should be emphasized that the estimated loads at the crack initiation were obtained by using the available strengths and fracture toughness reported in Krishnan and Xu (2011a). These parameters are approximate in nature due to the data scattering during experiments. Due to the lack of information on the dependence of the fracture toughness on the mode mixity ratio, the use of Eq. (23) to decompose the mode I and mode II fracture toughnesses is also approximate in nature. All these approximations can partially explain the difference between the estimated loads and the corresponding experimental data, nevertheless the order of magnitudes and trends are preserved.

6.4 Conclusion

The validation of the MA analysis requires the critical initiation crack length l_c to be small as compared with the other geometric parameters of the specimen, it is a posteriori observed that it holds true as expected. Therefore, the use of the asymptotic analysis seems reasonable. Interface crack initiation at V-notches along the adhesive bonding in bonded polycarbonate and PMMA subjected to mixed-mode loading conditions was investigated based on a combined experimental, FE and MA analysis. The V-notch specimens with an adhesive interface starting from its tip made at different notch angles were tested under three-point bending conditions. The experimental observations show that, due

to the weak adhesive bonding of the V-notched specimens in this investigation, the crack will emerge out of the bisector of the notch along the interface (even if $S = 0$ mm), which is defined as material-induced kinking by Xu and Rosakis (2003), whereas, if the interface is strong enough the crack will kink in the sheet in a direction that can be defined as load-induced kinking (Li and Xu 2007).

The load at the crack initiation increases when the notch angle increases. The computational results for the stress, stress intensity factor and energy release rate solutions for cracked and V-notched specimens based on the MA analysis are benchmarked with those based on the traditional FE analysis. The computational results are then used to explain and to correlate with the experimental data. A two-fold criterion developed by Leguillon (2002) that requires a simultaneous satisfaction of both energy and stress conditions for the crack initiation at a notch in the specimen of homogeneous brittle material is first extended for V-notch specimens under mixed-mode loading conditions and then used to estimate the loads at the crack initiation. The estimated loads appear to agree well with the experimental data.

Some experimental procedures to investigate the dependence of the fracture toughness on the mode mixity ratio for cracked specimens ($\omega = 0^\circ$) can be found in Wang and Suo (1990) and O'Dowd et al. (1992). As listed in Table 3, the values of the mode mixity ratio ψ are different for specimens with different notch angles ω under different loading positions S . Then it could be tempting to use an inverse method to estimate the values of the fracture toughness at different mode mixity ratios. An attempt was done in this direction but no clear trend could be found because resulting predictions were largely scattered.

A similar investigation for V-notch specimens of dissimilar materials will be reported in a future work.

Acknowledgments The financial support of this project by French National Centre for Scientific Research (CNRS) for VXT and DL is greatly appreciated. AK and LRX acknowledge the support from the US Office of Naval Research and the National Science Foundation.

References

- ABAQUS (2004) User's manual for version 6.5. ABAQUS, Providence
- Anderson TL (2004) Fracture mechanics fundamentals and applications, 3rd edn. CRC Press, FL

- Araki W, Nemoto K, Adachi T, Yamaji A (2005) Fracture toughness for mixed-mode I/II of epoxy resin. *Acta Mater* 53(3):869–875
- Caimmi F, Pavan A (2009) An experimental evaluation of glass-polymer interfacial toughness. *Eng Fract Mech* 76(18):2731–2747
- Dunn ML, Suwito W, Cunningham S (1997a) Fracture initiation at sharp notches: correlation using critical stress intensities. *Int J Solids Struct* 34(29):3873–3883
- Dunn ML, Suwito W, Cunningham S, May CW (1997b) Fracture initiation at sharp notches under mode I, mode II and mild mixed-mode loading. *Int J Fract* 84:367–381
- Garcia IG, Leguillon D (2012) Mixed-mode crack initiation at a v-notch in presence of an adhesive joint. *Int J Solids Struct* (to appear)
- Gomez FJ, Elices M, Berto F, Lazzarin P (2009) Fracture of V-notched specimens under mixed-mode (I+II) loading in brittle materials. *Int J Fract* 159:121–135
- Hashin Z (1996) Finite thermoelastic fracture criterion with application to laminate cracking analysis. *J Mech Phys Solids* 44:1129–1145
- Hutchinson J, Suo Z (1992) Mixed mode cracking in layered materials. *Adv Appl Mech* 29:63–191
- Krishnan A, Xu LR (2011a) Systematic evaluation of bonding strengths and fracture toughnesses of adhesive joints. *J Adhes* 87:1–19
- Krishnan A, Xu LR (2011b) A short-beam shear fracture approach to measure the mode II fracture toughness of materials with preferred interfaces. *Int J Fract* 169:15–25
- Krishnan A, Xu LR (2012) Experimental studies on the interaction among cracks, notches and interfaces of bonded polymers, submitted for publication
- Labossiere PEW, Dunn ML (1999) Stress intensities at interface corners in anisotropic bimetals. *Eng Fract Mech* 62:555–575
- Leguillon D (2002) Strength or toughness? A criterion for crack onset at a notch. *Eur J Mech A/Solids* 21:61–72
- Leguillon D, Sanchez-Palencia E (1987) Computation of singular solutions in elliptic problems and elasticity. Wiley, New York
- Leguillon D, Siruguet K (2002) Finite fracture mechanics—application to the onset of a crack at a bimaterial corner. In: Karihaloo BL (ed) IUTAM symposium on analytical and computational fracture mechanics of non-homogeneous materials, solid mechanics and its applications, vol 97. Kluwer, Dordrecht, pp 11–18
- Leguillon D, Yosibash Z (2003a) Failure at corners in brittle materials—validation of a criterion. In: 9th international conference on the mechanical behavior of materials, icm9, conference CD-ROM, Geneva (Swiss), May 25–29 2003
- Leguillon D, Yosibash Z (2003b) Crack onset at a v-notch. Influence of the notch tip radius. *Int J Fract* 122(1-2):1–21
- Leguillon D, Murer S, Recho N, Li J (2009) Crack initiation at a v-notch under complex loadings—statistical scattering. In: Proceedings of the international conference on fracture, ICF12, Ottawa, 12–17 July 2009
- Leguillon D (2011) Determination of the length of a short crack at a v-notch from a full field measurement. *Int J Solids Struct* 48:884–892
- Li XF, Xu LR (2007) T-Stresses across static crack kinking. *ASME J Appl Mech* 74:181–190
- O’Dowd NP, Shih CF, Stout MG (1992) Test geometries for measuring interfacial toughness. *Int J Solids Struct* 29(5):571–589
- Priel E, Bussiba A, Gilad I, Yosibash Z (2007) Mixed-mode failure criteria for brittle elastic V-notched structures. *Eng Fract Mech* 144:247–265
- Rice JR (1988) Elastic fracture mechanics concepts for interfacial cracks. *J Appl Mech* 55:98–103
- Seweryn A (1994) Brittle fracture criterion for structures with sharp notches. *Eng Fract Mech* 47:673–681
- Suo Z, Hutchinson JW (1990) Interface crack between two elastic layers. *Int J Fract* 43:1–18
- Taylor D, Cornetti P, Pugno N (2005) The fracture mechanics of finite crack extension. *Eng Fract Mech* 72:1021–1038
- Vu-Quoc L, Tran V-X (2005) Singularity analysis and fracture toughness-release rate for composites: piece-wise homogenous-anisotropic materials. *Comput Methods Appl Mech Eng* 195:5162–5197
- Wang JS, Suo Z (1990) Experimental determination of interfacial toughness using Brazil-nut-sandwich. *Acta Mech* 38:1279–1290
- Williams ML (1952) Stress singularities resulting from various boundary conditions in angular corners of plates in extension. *J Appl Mech* 19:526–528
- Xu L, Tippur HV (1995) Fracture parameters for interfacial cracks: an experimental-finite element study of crack tip fields and crack initiation toughness. *Int J Fract* 71:345–363
- Xu LR, Huang YY, Rosakis AJ (2003) Dynamic crack deflection and penetration at interfaces in homogenous materials: experimental studies and model predictions. *J Mech Phys Solids* 51:461–486
- Xu LR, Rosakis AJ (2003) An experimental study on dynamic failure events in homogenous layered materials using dynamic photoelasticity and high-speed photography. *Opt Laser Eng* 40:263–288
- Xu LR, Sengupta S, Kuai H (2004a) Dissimilar material joints with and without free-edge stress singularities: part I. A biologically inspired design. *Exp Mech* 44(6):608–615
- Xu LR, Sengupta S, Kuai H (2004b) An experimental and numerical investigation of adhesive bonding strengths of polymer materials. *Int J Adhes Adhes* 24:455–460
- Yosibash Z, Bussiba A, Gilad I (2004) Failure criteria for brittle elastic materials. *Int J Fract* 125(3-4):307–333
- Yosibash Z, Priel E, Leguillon D (2006) A failure criterion for brittle elastic materials under mixed-mode loading. *Int J Fract* 141(1):289–310